Evidence for Enhanced Tracer Diffusion in Soft Colloidal Glasses at Ultrahigh Packing

Zachary Fink [§], Paul Y. Kim [‡], Satyam Srivastava [§], Alexander E. Ribbe [§], David A. Hoagland[§], and Thomas P. Russell [*§‡†]*

AUTHOR ADDRESS

§ Polymer Science and Engineering Department, University of Massachusetts Amherst, Amherst, Massachusetts 01003, United States

‡ Materials Sciences Division, Lawrence Berkeley National Laboratory, Berkeley, California 94720, United States

† Advanced Institute for Materials Research (WPI-AIMR), Tohoku University, 2-1-1 Katahira, Aoba, Sendai 980-8577, Japan

ABSTRACT

Nearly monodisperse nanoparticle spheres attached to a nonvolatile ionic liquid surface were tracked by *in-situ* scanning electron microscopy to obtain the tracer diffusion coefficient D_{tr} as a function of areal fraction, ϕ. The *in-situ* technique resolved both tracer (gold) and background (silica) particles for a period of ~1-2 minutes, highlighting their mechanisms of diffusion, which were strongly dependent on ϕ. Assembly structure and dynamics trends at low and moderate ϕ paralleled those reported for larger colloidal spheres, showing an increase in order and a decrease in D_{tr} by over four orders of magnitude. However, ligand interactions are more important near jamming, and lead to different caging and jamming dynamics for NPs. The normalized D_{tr} at ultrahigh ϕ depended on particle diameter and ligand molecular weight.

Increasing the PEG molecular weight by a factor of four increased D_{tr} by two orders of magnitude at ultrahigh ϕ, indicating stronger ligand lubrication for smaller particles.

KEYWORDS: electron microscopy, single particle tracking, colloidal glasses, nanoparticles, diffusion coefficient, ionic liquid

Transitions of particle packings from low density states, in which particles are disordered and highly mobile, to high density states, in which particle assemblies are glassy, jammed, or crystalline and nearly immobile, have long been a focus of materials science.[1-12] For small, well-dispersed particles, ordering improves as particle density increases, accompanied by a shift from dominantly single-particle dynamics to multiple-particle or cooperative dynamics. In a broad scope, understanding the particle assembly mechanisms and associated structural transitions can impact numerous nanotechnologies, including bicontinuous jammed emulsions (bijels),[13] emulsion encapsulation,[14, 15] high throughput chemical Picker emulsion catalysts,[16] and high density photonic assemblies for optoelectronic devices.[17] Directly visualizing NP dynamics in these contexts could have far-reaching consequences for medicine, composite mechanics, electrical devices, and sensors.[13-15, 18-20]

An important aspect of these dynamics is the tracer diffusion coefficient D_{tr}, which was measured here for nanoparticles (NPs) dispersed on a liquid surface across the full range of surface areal density ϕ. These measurements were facilitated by our recently developed scanning electron microscopy (SEM) method that offers *in situ* 'open' single particle imaging of NPs residing on an ionic liquid (IL) surface.[21-23] The local details of the assemblies can be visualized

by SEM, a powerful advantage over optical microscopy, which can only track large particles.[24-27] The behaviors of NPs and colloidal particles are distinct, due to the different relative length scales of interparticle interactions, which for NPs may extend over distances comparable to or greater than the particle diameter *d*. This difference in interaction length scales means that jamming and caging behavior of NPs may be radically different than larger spheres. Adding ligands to the NPs further complicates these interactions and may lead to interesting and unexpected behavior as these interactions become more important near jamming. The exquisite detail afforded by this SEM approach allows direct visual access to dense NP packings, where we hypothesize stabilizing ligands on the NPs can greatly affect NP dynamics, especially at ultrahigh ϕ.

Similar interfacial particle systems have previously been studied by ensemble-average methods, including microrheology,[2, 28-30] grazing incidence or small angle x-ray scattering and reflectivity,[31-33] Langmuir-Blodgett techniques,[32, 34, 35] and thermal approaches[9, 29] yielding important insights into the density-driven transitions of two-dimensional NP packings. However, these methods cannot follow the simultaneous changes to organization and motion of individual NPs or NP packing heterogeneities. Another distinct advantage of our SEM method is that the NP motions are restricted to the 2D interface, which allows for increased fidelity in tracking without concern of diffusion out of plane. Less traditional imaging methods such as liquid cell TEM,[36-38] liquid AFM,[39] super-resolution optical microscopy,[40-42] and variable pressure SEM have been used to visualize such nanoscale assemblies, but have weaknesses in their geometrical constraints, spatiotemporal resolution, or artefacts induced from outside perturbations. SEM imaging circumvents these problems by taking advantage of the negligible vapor pressure and

innate conductivity of ILs which enables large scale open imaging of the liquid surface without evaporation or charging.

The diffusion and packing of small spheres at a liquid surface have been examined frequently,[25-27, 43-57] with studies variously focused on impacts of contact angle, interfacial fluid dynamics, interfacial tension, and changes in interfacial viscosity. In the present study D_{tr} was measured by SEM for PEGylated tracer gold NP spheres as a function of ϕ, tracking NP motions/ displacements at an IL-vacuum interface containing a backdrop of neighboring silica NPs with 5,000 g/mol PEG ligands. The orientational ($<\psi_6>$) and translational (T^*) order parameters of the NPs and the pair correlation function were determined for all ϕ.[21-23, 58, 59] Previous studies of sphere diffusion at liquid surfaces typically used larger particles and nearly all are terminated at densities well below jamming, limiting the variation of D_{tr} measured and missing any phenomena close to jamming. Archer *et al.* studied similar soft colloidal glasses in the bulk at ultrahigh ϕ, and showed that these suspensions can counter NP jamming under the appropriate conditions (*e.g.* NP diameter to ligand size ratio).[60, 61] Our SEM method uniquely positions us to visualize tracer NP diffusion across all ϕ and uncover the role ligands play at ultrahigh ϕ.

When dispersed on the IL (Ethyl-3-methylimidazolium ethyl sulfate) interface at lowϕ, the NPs displayed 2D interactions closely resembling those of hard spheres.[21, 23] Although their ligand configurations could not be characterized *in-situ*, small angle neutron scattering of PEG dissolved in similar ILs yielded a Flory exponent of 0.55-0.60,[62] suggesting moderate-to-good solvent conditions. Salerno and coworkers examined PEGylated NPs,[63] and their modeling indicated that a 5,000 g/mol PEG ligand layer was ~2-3 nm thick in a good solvent. A 5-nm correction was thereby made to d in calculating ϕ, which was most robust at low ϕ where NP-NP

contacts were infrequent. At high ϕ, ligand-ligand interactions were prevalent, so the ligand coronae were likely compressed. In these cases, the Alexandre-deGennes brush model better approximates the interparticle potential.[22, 64]

Each tracer NP was matched to a non-tracer NP of nearly the same *d*, and the matched pair are referenced by their nominal diameter expressed in nanometers, 100 (for 101-nm *d*), 130 (for 132-nm *d),* 160 (for 158-nm *d*), and 240 (for 238-nm *d*). Tracer particles are used, since the NPs can displace a distance greater than their center-center spacing in the time between frames for moderate-to-high ϕ packings and could not be distinguished, a problem avoided with the tracer NP strategy. All NPs had less than ~11-13% dispersity in *d*, and all bore the same dense PEG ligand layer, which drove the NPs to the IL surface due to the low surface energy of PEG, ~43 mN/m, compared to that of IL, ~48 mN/m.[23] The ligand layer thickness for all samples was much less than *d*, so the layers primarily acted as non-sticky short-range "bumpers", precluding aggregation of NPs in the liquid or at its surface. The PEG ligands also afford all the particles with the same surface chemistry and same contact angle, and nothing indicated that the interior compositional difference between tracer and background NPs affected their interactions. Figure 1 shows NPs in a monolayer, prepared as described in the Methods section, as the drop volume was manipulated for ϕ close to NP jamming. Precise control over ϕ is directed by the increase/decrease of the IL volume, which changes the total surface area of the droplet (*e.g.,* when IL is added ϕ decreases, and when IL is removed ϕ increases). NP arrangements before and after the ϕ change were indistinguishable, establishing structural reversibility upon interfacial expansion/compression and a means to increase ϕ.

Tracking was performed in a similar manner to our previous work.[21-23, 58] Briefly, imaging was performed at room temperature near the drop apex to minimize the impact of interfacial curvature on NP motion as well as the distortions emanating from 2D imaging of a curved interface. Although the mobility of Au tracer particles is impacted by the difference in particle density, gold coated silica NP tracers can be used, so the small difference in inertia is minor. The interfacial NPs, due to their small masses, did not produce gravity-induced menisci, and the IL surface surrounding them was, therefore, nearly planar. To maintain the ~14° contact angle θ under this constraint,[21] NP centers lay well below the surface. Since SEM secondary electron imaging mode reveals only the topmost 20-50 nm of surface structure,[23] the more deeply submerged portions of NPs, including NP-NP contacts, were not visualized, and the NPs appeared as white circular caps surrounded by a dark, continuous IL matrix (Figure 1). Further details on the imaging protocol can be found in the Supporting Information.

Figure 2a presents typical SEM-imaged trajectories of 160 nm NPs for ϕ equal to 0.78, 0.65, and 0.33. Initially, all tracers displayed time-invariant irregular motions. At ϕ=0.78, these motions were mostly caged over the period monitored, rendering the trajectories much more compact than those at lower ϕ. Intermittent caging is evident at ϕ=0.65, whereas no caging is noted at ϕ=0.33. Movies underlying the trajectories of Figure 2a are provided in Supporting Information movies SM1-SM3, while Figures S2-S5 offer images for several d and ϕ along with associated movies (SM4-SM6). SM7 provides snapshots of a continuous increase in ϕ using 160 nm NPs. While successive frames could be captured over thousands of seconds, NP motions beyond ~100s time steps could display an inconsistent slowing down of dynamics, a feature attributed to beam-induced IL crosslinking from radiolysis. Lowering beam current and

increasing scan speed decreases the crosslinking, but imaging contrast and quality would concurrently diminish. Except at ϕ close to jamming, the initial period of stable dynamics was long enough to capture NP excursions comparable or larger than d.

At least three independent measurements and fifteen individual NP trajectories, such as those in Figure 2a, were used to construct mean square displacement $\langle r^2 \rangle$ vs. time lag τ for each d and ϕ. Figure 2b provides plots of $\langle r^2 \rangle$ vs. τ for ϕ=0.55 for all d, and as anticipated for semidilute ϕ, $\langle r^2 \rangle$ decreased as d increased, indicating decreased mobility. The inset shows the same data in terms of normalized variables $\langle r^2 \rangle / d^2$ and $\tau D_{tro}/d^2$, where D_{tro} is D_{tr} for an infinity dilute system (*i.e.* ϕ approaches zero, see Figure 4). The data collapse and show a slope close to unity with reasonable linearity, since the underlying dynamics are scale invariant. These results are consistent with the analogous normalized data for larger hard sphere colloids.[26] Deviations, especially at longer times for large ϕ are attributed caging effects. Figure 2b presents $\langle r^2 \rangle$ vs. τ for 130 nm NPs, and shows the transition from ordinary but congested Brownian motion to persistently caged Brownian motion, which is vaguely reflected in the significant drop in $\langle r^2 \rangle$ for $\phi \gtrsim 0.65$. When ϕ rose above $\phi \eqsim 0.70$, approximately the onset of 2D colloidal crystalline ordering, the characteristic time for NP escape from cages became significantly greater than the characteristic time d^2/D_{tro} than at slightly lower ϕ, reflecting a sharp break toward short-term diffusion (inset Figure 2b). Caging is visually obvious in all NP trajectories collected for $\phi \gtrsim 0.65$, and in the $\langle r^2 \rangle$ vs. τ plots. Figures S6-S9 display the analogous plots for all d across the same ϕ range alongside fits to Fickian and Fickian with drift models (Supporting Information) for calculating D_{tr}. While some of these trends are unsurprising, they validate that real-time *in-situ* SEM tracking can provide D_{tr} for interfacial NPs.

The ϕ-dependence of D_{tr} will coincide with changes in NP organization, which SEM captured across all ϕ. To characterize organization, the centers of background NPs were first obtained by procedures essentially the same as for tracer NPs (see Methods). Delaney triangulation then produced Voronoi diagrams from which the hexagonal orientational order parameter $<\psi_6>$, translational order parameter T^*, number of nearest neighbors z, and pair correlation function $g(r)$ were calculated.[22, 59, 65] Figure 3a-3d provide the first two of these characterizations for 160 nm NPs at ϕ equal to 0.33 and 0.80, and Figure 3e and Figure S10 offer the other characterizations for $0.1 \leq \phi \leq 0.83$. Across all ϕ, NP organization was fully consistent with literature reports for 2D sphere packings,[59, 64, 66] with hexatic and crystal phases observed at conditions expected for hard spheres.

For 2D Brownian motion conforming to Fick's law, D_{tr} is calculated from the slope of $<r^2>$ vs τ, and analyzing NP tracking data in terms of Eqs. S1 and S2, Figures 4a and 4b offer D_{tr} as a function of ϕ for all d. Unsurprisingly given the trends discussed for Figure 2, all ϕ show about one order of magnitude decrease in D_{tr} before ordering, while four orders of magnitude decrease is incurred afterward. Similar observations have been made by Dozier *et al.*[67] for electrostatically repelling colloids in the bulk. However, the SEM method is able to resolve tracer NP positions to ±10 nm over a Fickian diffusion period lasting ~100s, and D_{tr} as small as $\sim 5 \times 10^{-7}$ $\mu m^2/s$ could be measured. Thus, D_{tr} could be assessed for fully caged but unjammed (jamming emerges at $\phi \backsimeq 0.82\text{-}0.85$)[44, 57, 65] NPs at $\phi \gtrsim 0.70$, precisely where Archer *et al.* predicted liquid-like jamming behavior.[60, 61] In the log-linear format of Figure 4b, the D_{tr} at ultrahigh ϕ is highlighted and displays an inflection point with a d-dependance that would not be expected with only hard

sphere interactions. In this case, the normalized data in the inset of Figure 4b should superimpose across all ϕ, and is met for all ϕ except in the highest ϕ region.

In many contexts a semi-empirical model for D_{tr} can be helpful in distinguishing subtle effects immediately prior to the onset of ordering. For an isolated hard sphere diffusing at a planar fluid interface, D_{tr} can be expressed in a modified Stokes-Einstein form,

$$D_{tr}=\frac{32\,k_B T}{3\pi\eta_o d\left[16+9\cos\theta-2.224\cos^2\theta+O\left(\cos^3\theta\right)\right]} \tag{1}$$

following calculations from Dörr *et al.*[53] analytically determined *via* a geometric perturbation approach. Here k_B is the Boltzmann constant, T is the temperature, and η_o is the fluid viscosity. For a ligand-decorated NP surface, η_o depends on ϕ and could further depend on the spreading/interaction of ligands, especially approaching jamming. For a bulk suspension of hard spheres, the Krieger-Dougherty model[54] closely tracks the volume fraction ϕ dependence of suspension viscosity,

$$\eta_o=\eta\left(1-\frac{\phi}{\phi_{max}}\right)^{-B} \tag{2}$$

where η is the IL viscosity, ϕ_{max} is the maximum achievable volume fraction, and B is an empirical exponent. Setting ϕ_{max} to the inflection point (ϕ=0.76), constraining B to a single value (=3/2 for 2D interfaces), and substituting Eq. 2 into Eq. 1, produces the solid curves drawn through the data sets as shown in Figure S11. Until ϕ approaches the ordering transition, agreement between curves and data is surprisingly good, but loses accuracy for low d and high ϕ. Interestingly, when B is adjusted to fit the data separately for each d, values of 1.5, 1.45, 1.35,

and 1.2 are obtained in the order of descending d (fits in Figure 4). This decreasing trend in exponent value may be related to increased ligand lubrication and decreased interfacial viscosity.

The D_{tr} dependence on d before ordering is attributed to defect annihilation near jamming. The packing of background NPs was initially decorated with numerous defects, vacancies, and grain boundaries prior to ordering, and showed that defects along grain boundaries were increasingly annihilated across $0.73<\phi<0.78$, exactly where normalized D_{tr} fell most abruptly. The d-dependence of D_{tr}/D_{tro} above the inflection point cannot be explained by the same argument. This dependence must arise from ligand-mediated NP interactions since packing defects were rare, and diffusion within cages prevailed. In this scenario, the ratio of ligand thickness to NP size becomes important, and NPs can no longer be treated as hard spheres. Under these circumstances, Figure 4b shows that D_{tr}/D_{tro} declined as the ratio of d to ligand layer thickness increased. For smaller d NPs, ligands fill a larger fraction of the interstitial area between NPs, and consequently, can better lubricate displacements when the NPs are nearly in contact. Archer *et al.* reported that neat, ligand-coated NPs can even flow as bulk liquids, demonstrating that appropriate ligands can counter NP jamming in three-dimensional sphere packings.[60, 61] If the same holds for these 2D monolayers, D_{tr}/D_{tro} is sensitive to ligand chemistry, ligand length, and ligand grafting density at $\phi \gtrsim 0.76$.

To highlight the impact the ligand length has on the observed dynamics, 100 nm NPs were functionalized with 20,000 g/mol PEG ligands. The 4 times increase in ligand length is expected to increase the ligand layer by ~2.3 times ($4^{3/5}$), indicating a roughly 5.75 nm brush, which was used in the calculation of the packing fractions. Supporting movie SM8 shows the motion of 100 nm particles with 20k ligands at $\phi = 0.8$. In comparison to the motion of the same size particle,

but with 5k ligand (SM9) the increase in diffusion is visually apparent. To quantitatively distinguish the difference in D_{tr}, $\langle r^2 \rangle$ was obtained for the 20k PEGylated NPs and compared to their 5k counterparts. Figure 5a shows the $\langle r^2 \rangle$ obtained for ultrahigh ϕ = 0.8, and show a significant increase in slope by two orders of magnitude, corresponding to an increase in diffusion from ~5.94 x 10^{-6} $\mu m^2/s$ for the 5k PEGylated NPs to 8.75 x 10^{-4} $\mu m^2/s$ for the 20k PEGylated NPs. The larger ligand molecular weight drastically improves the lubricated motion of the NPs and results in the enhanced diffusion of the NPs. Figure 5b shows the same comparison between the 20k and 5k PEGylated NPs, but at ϕ=0.33, and there was no significant change in the measured D_{tr}. These findings suggest that ligand effects can impact NP dynamics above $\phi \gtrsim 0.76$, with little effect below the onset of jamming.

Before availability of this SEM method, NP tracking at non-dilute conditions in or on liquids was problematic. The tracer method used here has provided quantitative insights into diffusion processes across the full range of ϕ, highlighting the different behavior observed for small NPs at ultrahigh ϕ. A decrease in D_{tr} by five orders of magnitude was found, with the largest impact noted at ϕ too high for visualization/tracking by any other method. The same approach can be applied to smaller spheres, d<100 nm, where ligand lubrication is expected to be even greater, but additional imaging refinements and better understanding of beam artefacts, will be needed to improve contrast.

While dense NP assemblies display many properties analogous to those of larger particles, they also possess their own characteristic features; for example, NPs typically are coated with ligand layers thick enough to greatly impact dynamics as was uncovered here, and evidenced by the increased D_{tr} from ligand lubrication at ultrahigh ϕ. This increase in particle mobility was

highlighted for larger 20,000 g/mol PEGylated NPs, which resulted in a two-order magnitude increase in D_{tr} for 100 nm NPs. Chemically and structurally more interesting ligands can be chosen (telechelic, block copolymer, branched, *etc*.) to create entirely new interactions and ordering, providing a host of phenomena otherwise outside the realm of single particle visualization methods. Further optimization of imaging methods and the implementation of mixed systems (*i.e.* spheres, rods, cubes, *etc.*) will also allow for time-evolving compositional and alignment variations at the nanoscale, which may greatly improving our understanding of structural variations in existing and future nanotechnologies.

FIGURES

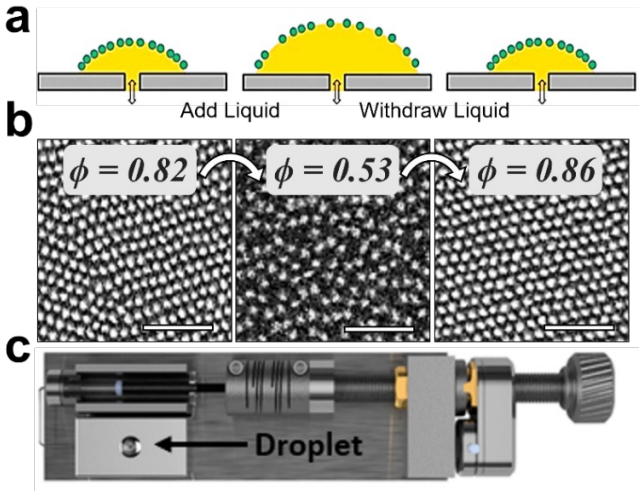

Figure 1. SEM liquid cell. (a) Sequential addition/withdrawal of liquid to adjust drop size; (b) SEM images of NP arrangements after addition/withdrawal of liquid from drop. Initial and final arrangements are nearly jammed (scale bars: 1 μm); and (c) Liquid cell component layout displaying specimen stage and supported drop (lower left), motorized syringe (upper right), and connecting fluid path (upper left).

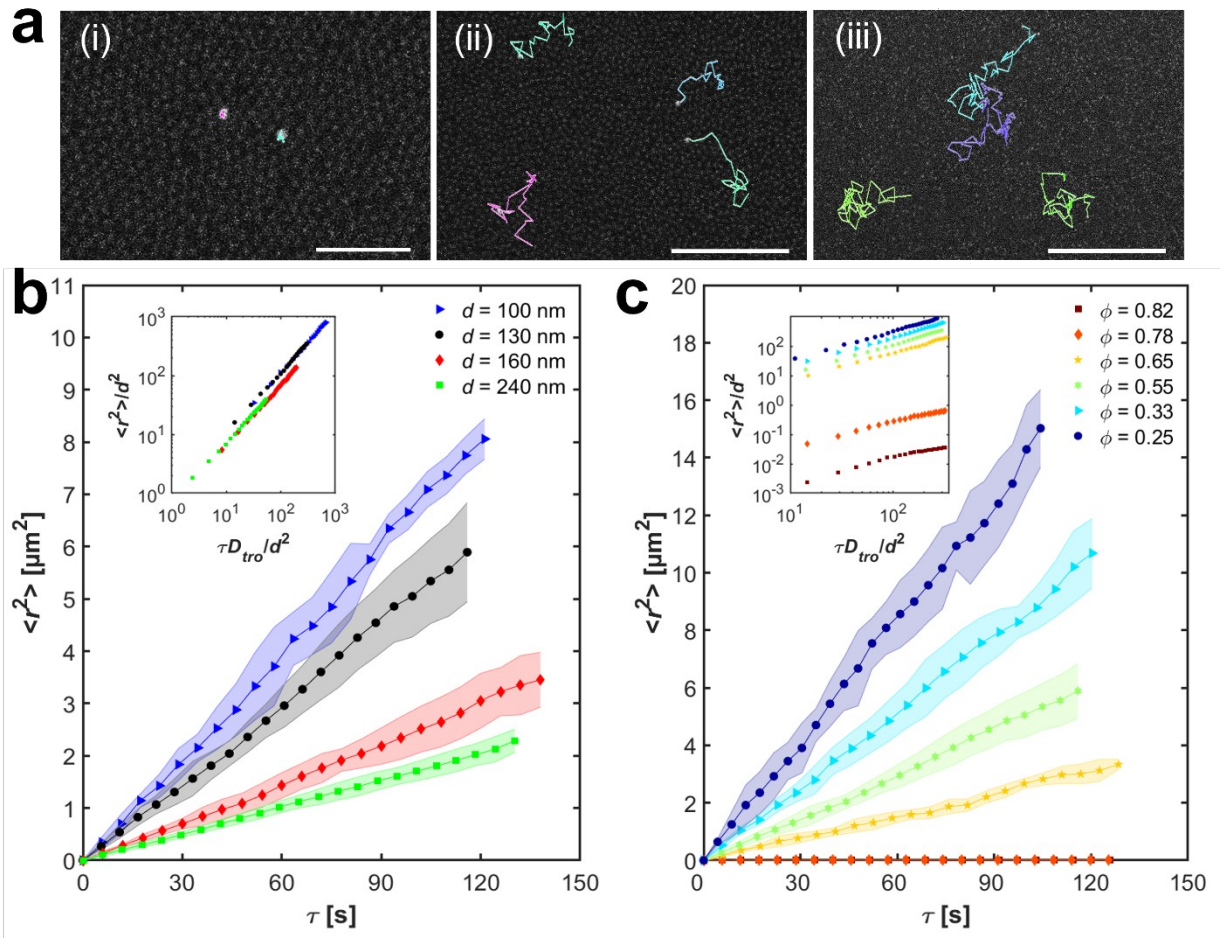

Figure 2. (a) Trajectories of 160 NPs for ϕ = (i) 0.78, (ii) 0.65, and (iii) 0.33. As reflected by scale bars of (a) 1 μm, (b) 3 μm, and (c) 5 μm, magnification was adjusted to highlight NP motion. (b) Mean-square-displacement $\langle r^2 \rangle$ vs. time lag τ for all d at ϕ ~0.55 and (c) select ϕ for d=130 nm. Insets show the same data normalized by the characteristic length scale d and time scale $d^2/D_{tro.}$

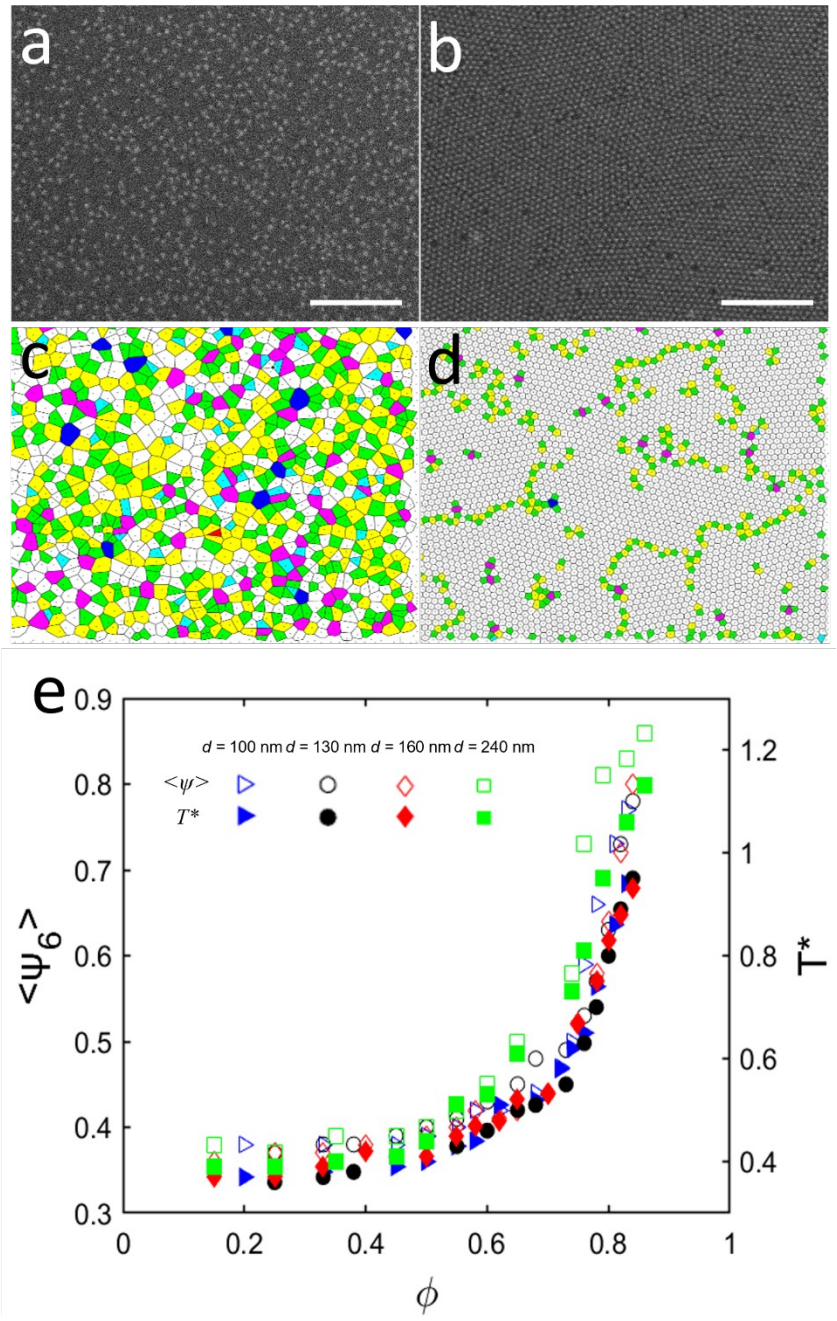

Figure 3. SEM image of 160 NPs at (a) ϕ = 0.33, and (b) ϕ = 0.80. Scale bars: 2 μm. Corresponding Voronoi Tessellations (c) and (d) for SEM images in (a) and (b). Color map: z=3 (red), 4 (light blue), 5 (green), 6 (white), 7 (yellow), 8 (pink), and 9 (dark blue). (e) Order parameters $<\psi_6>$ (closed symbols) and T^* (open symbols) for all d as a function of ϕ, showing good overlap and an upturn at $\phi \approx 0.72$-0.76; 100, 130, 160, and 240 NPs are represented by blue triangles, black circles, red diamonds, and green squares, respectively.

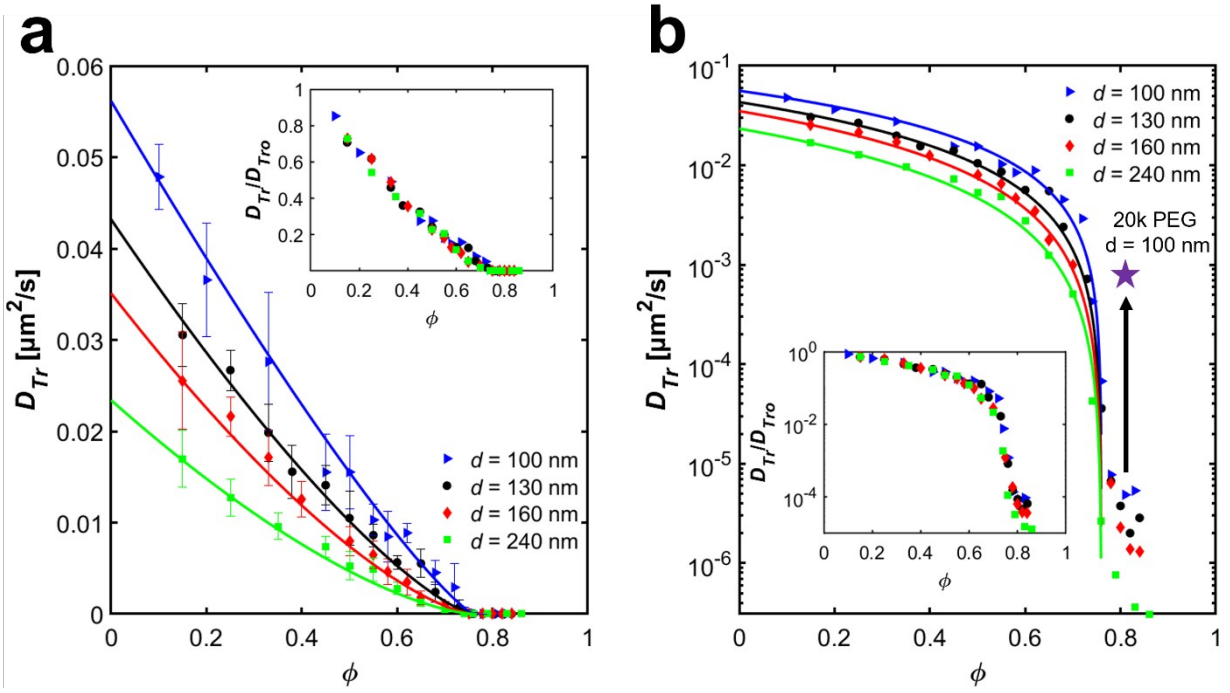

Figure 4. D_{tr} as a function of ϕ for all d. (a) Data are displayed in linear-linear format in the main plot, and the inset shows the same data plotted in linear-linear format after D_{tr} is divided D_{tro}. (b) Data are displayed in log-linear format in the main plot, and the inset shows the data displayed in log-linear format after the same division of D_{tr}. The division collapses the ϕ dependence except at large ϕ. The data are fit to a phenomenological model provided by Dörr *et al.* (see Eq. 1).

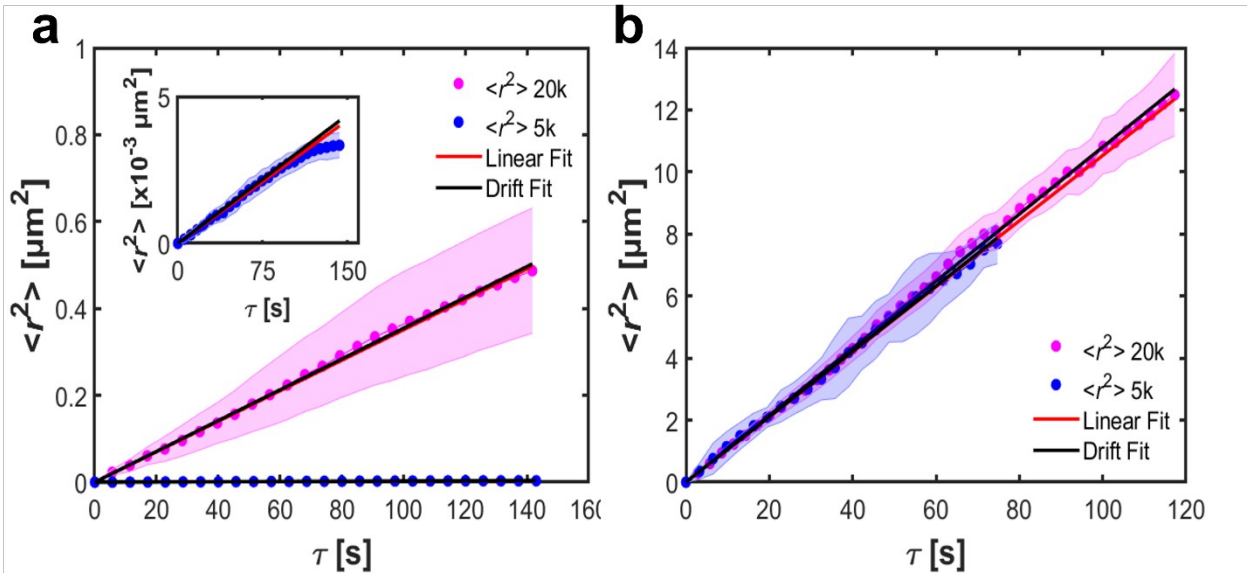

Figure 5. $\langle r^2 \rangle$ vs. τ for 100 nm NPs at (a) $\phi = 0.8$ and (b) $\phi = 0.33$ for both 5k (blue) and 20k (magenta) PEG ligands with fits to extract D_{tr}. Inset shows the zoomed in $\langle r^2 \rangle$ vs. τ for the 5k PEG ligands.

ACKNOWLEDGMENT

We acknowledge the financial support of the National Science Foundation through DMR-2104883. In depth analysis of NP packings by PYK and TPR was supported by the U.S. Department of Energy, Office of Science, Office of Basic Energy Sciences, Materials Sciences and Engineering Division under Contract No. DE-AC02-05-CH11231 within the Adaptive Interfacial Assemblies Towards Structuring Liquids program (KCTR16).

ASSOCIATED CONTENT

Supporting Information

The following files are available free of charge.

Text describes NP and ligand interactions at the interface and detailed sample preparation and imaging conditions. Mean square displacement equations for Brownian diffusion and diffusion with drift models are provided. Nanoparticle organization and structure are described using the hexagonal orientational order parameter $\langle\psi 6\rangle$, the translational order parameter T^*, and the pair correlation function $g(r)$. Figure S1, TEM images of tracer NPs used; Figure S2, snapshots of 100 nm NPs in a zoomed in area of different ϕ ; Figure S3, snapshots of 130 nm NPs in a zoomed in area of different ϕ; Figure S4, snapshots of 160 nm NPs in a zoomed in area of different ϕ; Figure S5, snapshots of 240 nm NPs in a zoomed in area of different ϕ; Figure S6, Mean-square-displacement $\langle r^2\rangle$ vs. time lag τ for 100 nm NPs; Figure S7, Mean-square-displacement $\langle r^2\rangle$ vs. time lag τ for 130 nm NPs; Figure S8, Mean-square-displacement $\langle r^2\rangle$ vs. time lag τ for 160 nm NPs; Figure S9, Mean-square-displacement $\langle r^2\rangle$ vs. time lag τ for 240 nm NPs; Figure S10, number of nearest neighbors and pair correlation function analysis for all 160

NPs. Figure S11, D_{tr} as a function of ϕ for all d fit using equations 1 and 2 where B=3/2; Supporting movies SM 1-3 show diffusion of 160 nm NPs, while SM 4-6 show various other ϕ and d. SM 7 shows snapshots of a continuous increase in ϕ using 160 nm NPs. SM 8 shows the motion of 100 nm NPs with 20k ligands at ϕ = 0.8, while SM 9 shows the motion of 100 nm NPs with 5k ligands at ϕ = 0.8.

AUTHOR INFORMATION

Corresponding Author

* Thomas P. Russell, E-mail: russell@mail.pse.umass.edu.

* David A. Hoagland, E-mail: hoagland@mail.pse.umass.edu

Author Contributions

Zachary Fink: conceptualization, investigation, formal analysis, methodology, writing- original draft, and writing – review and editing. Paul Kim: methodology, software, and writing – review and editing. Satyam Srivastava: investigation and writing – review and editing. Alexander Ribbe: methodology, resources, and writing – review and editing. David Hoagland: conceptualization, funding acquisition, supervision, resources, and writing – review and editing. Thomas Russell: conceptualization, funding acquisition, supervision, resources, and writing – review and editing. The manuscript was written through contributions of all authors.

REFERENCES

(1) Courtland, R. E.; Weeks, E. R. Direct Visualization of Ageing in Colloidal Glasses. *J. Phys. Cond. Mat.,* **2003**, *15*, S359-S365.

(2) Crocker, J. C.; Valentine, M. T.; Weeks, E. R.; Gisler, T.; Kaplan, P. D.; Yodh, A. G.; Weitz, D. A. Two-Point Microrheology of Inhomogeneous Soft Materials. *Phys. Rev. Lett.,* **2000**, *85*, 888-891.
(3) Edmond, K. V.; Elsesser, M. T.; Hunter, G. L.; Pine, D. J.; Weeks, E. R. Decoupling of Rotational and Translational Diffusion in Supercooled Colloidal Fluids. *Proc. Natl. Acad. Sci. U. S. A.,* **2012**, *109*, 17891-17896.
(4) Garbin, V.; Crocker, J. C.; Stebe, K. J. Nanoparticles at Fluid Interfaces: Exploiting Capping Ligands to Control Adsorption, Stability and Dynamics. *J. Colloid Interface Sci.,* **2012**, *387*, 1-11.
(5) Hunter, G. L.; Weeks, E. R. The Physics of the Colloidal Glass Transition. *Rep. Prog. Phys.,* **2012**, *75*, 066501.
(6) Isa, L.; Kumar, K.; Muller, M.; Grolig, J.; Textor, M.; Reimhult, E. Particle Lithography from Colloidal Self-Assembly at Liquid-Liquid Interfaces. *ACS Nano,* **2010**, *4*, 5665-5670.
(7) Lin, X. M.; Jaeger, H. M.; Sorensen, C. M.; Klabunde, K. J. Formation of Long-Range-Ordered Nanocrystal Superlattices on Silicon Nitride Substrates. *J. Phys. Chem. B,* **2001**, *105*, 3353-3357.
(8) Ni, R.; Stuart, M. A. C.; Dijkstra, M.; Bolhuis, P. G. Crystallizing Hard-Sphere Glasses by Doping with Active Particles. *Soft Matter,* **2014**, *10*, 6609-6613.
(9) Peng, Y.; Wang, Z.; Alsayed, A. M.; Yodh, A. G.; Han, Y. Melting of Colloidal Crystal Films. *Phys. Rev. Lett.,* **2010**, *104*, 205703.
(10) Pieranski, P. Two-Dimensional Interfacial Colloidal Crystals. *Phys. Rev. Lett.,* **1980**, *45*, 569-572.
(11) Tanaka, H.; Kawasaki, T.; Shintani, H.; Watanabe, K. Critical-Like Behaviour of Glass-Forming Liquids. *Nat. Mater.,* **2010**, *9*, 324-331.
(12) Weeks, E. R.; Weitz, D. A. Properties of Cage Rearrangements Observed near the Colloidal Glass Transition. *Phys. Rev. Lett.,* **2002**, *89*, 095704.
(13) Haase, M. F.; Stebe, K. J.; Lee, D. Continuous Fabrication of Hierarchical and Asymmetric Bijel Microparticles, Fibers, and Membranes by Solvent Transfer-Induced Phase Separation (Strips). *Adv. Mater.,* **2015**, *27*, 7065-7071.
(14) Strong, L. E.; West, J. L. Thermally Responsive Polymer-Nanoparticle Composites for Biomedical Applications. *Wiley Interdiscip. Rev: Nanomed. Nanobiotechnol.,* **2011**, *3*, 307-317.
(15) Sullivan, A. P.; Kilpatrick, P. K. The Effects of Inorganic Solid Particles on Water and Crude Oil Emulsion Stability. *Ind. Eng. Chem. Res.,* **2002**, *41*, 3389-3404.
(16) Kaang, B. K.; Mestre, R.; Kang, D. C.; Sanchez, S.; Kim, D. P. Scalable and Integrated Flow Synthesis of Triple-Responsive Nano-Motors Via Microfluidic Pickering Emulsification. *Appl. Mater. Today,* **2020**, *21*, 100854.
(17) Yadav, A.; Gerislioglu, B.; Ahmadivand, A.; Kaushik, A.; Cheng, G. J.; Ouyang, Z. B.; Wang, Q.; Yadav, V. S.; Mishra, Y. K.; Wu, Y. L.; Y. Liu; S. RamaKrishna,. Controlled Self-Assembly of Plasmon-Based Photonic Nanocrystals for High Performance Photonic Technologies. *Nano Today,* **2021**, *37*, 101072.
(18) Dinsmore, A. D.; Hsu, M. F.; Nikolaides, M. G.; Marquez, M.; Bausch, A. R.; Weitz, D. A. Colloidosomes: Selectively Permeable Capsules Composed of Colloidal Particles. *Science,* **2002**, *298*, 1006-1009.

(19) Lv, Y.; Du, Y.; Qiu, W. Z.; Xu, Z. K. Nanocomposite Membranes Via the Codeposition of Polydopamine/Polyethylenimine with Silica Nanoparticles for Enhanced Mechanical Strength and High Water Permeability. *ACS Appl. Mater. Interfaces,* **2017**, *9*, 2966-2972.
(20) Stratford, K.; Adhikari, R.; Pagonabarraga, I.; Desplat, J. C.; Cates, M. E. Colloidal Jamming at Interfaces: A Route to Fluid-Bicontinuous Gels. *Science,* **2005**, *309*, 2198-2201.
(21) Kim, P. Y.; Gao, Y. G.; Chai, Y.; Ashby, P. D.; Ribbe, A. E.; Hoagland, D. A.; Russell, T. P. Assessing Pair Interaction Potentials of Nanoparticles on Liquid Interfaces. *ACS Nano,* **2019**, *13*, 3075-3082.
(22) Kim, P. Y.; Gao, Y. G.; Fink, Z.; Ribbe, A. E.; Hoagland, D. A.; Russell, T. P. Dynamic Reconfiguration of Compressed 2d Nanoparticle Monolayers. *ACS Nano,* **2022**, *16*, 5496-5506.
(23) Kim, P. Y.; Ribbe, A. E.; Russell, T. P.; Hoagland, D. A. Visualizing the Dynamics of Nanoparticles in Liquids by Scanning Electron Microscopy. *ACS Nano,* **2016**, *10*, 6257-6264.
(24) Crocker, J. C.; Grier, D. G. Methods of Digital Video Microscopy for Colloidal Studies. *J. Colloid Interface Sci.,* **1996**, *179*, 298-310.
(25) Lin, B. J.; Chen, L. J. Phase Transitions in Two-Dimensional Colloidal Particles at Oil/Water Interfaces. *J. Chem. Phys.* **2007**, *126*, 034706.
(26) Thorneywork, A. L.; Rozas, R. E.; Dullens, R. P. A.; Horbach, J. Effect of Hydrodynamic Interactions on Self-Diffusion of Quasi-Two-Dimensional Colloidal Hard Spheres. *Phys. Rev. Lett.,* **2015**, *115*, 268301.
(27) Weeks, E. R.; Weitz, D. A. Subdiffusion and the Cage Effect Studied near the Colloidal Glass Transition. *Chem. Phys.,* **2002**, *284*, 361-367.
(28) Cicuta, P.; Stancik, E. J.; Fuller, G. G. Shearing or Compressing a Soft Glass in 2d: Time-Concentration Superposition. *Phys. Rev. Lett.,* **2003**, *90*, 236101.
(29) Fukushima, T.; Kosaka, A.; Ishimura, Y.; Yamamoto, T.; Takigawa, T.; Ishii, N.; Aida, T. Molecular Ordering of Organic Molten Salts Triggered by Single-Walled Carbon Nanotubes. *Science,* **2003**, *300*, 2072-2074.
(30) Orsi, D.; Baldi, G.; Cicuta, P.; Cristofolini, L. On the Relation between Hierarchical Morphology and Mechanical Properties of a Colloidal 2d Gel System. *Colloid Surf. A,* **2012**, *413*, 71-77.
(31) Als-Nielsen, J.; Kjær, K. X-Ray Reflectivity and Diffraction Studies of Liquid Surfaces and Surfactant Monolayers. In *Phase Transitions in Soft Condensed Matter*, Riste, T., Sherrington, D. Eds.; Springer US, 1989; pp 113-138.
(32) Kubowicz, S.; Hartmann, M. A.; Daillant, J.; Sanyal, M. K.; Agrawal, V. V.; Blot, C.; Konovalov, O.; Mohwald, H. Gold Nanoparticles at the Liquid-Liquid Interface: X-Ray Study and Monte Carlo Simulation. *Langmuir,* **2009**, *25*, 952-958.
(33) Wu, L. L.; Wang, X.; Wang, G.; Chen, G. In Situ X-Ray Scattering Observation of Two-Dimensional Interfacial Colloidal Crystallization. *Nat. Commun.* **2018**, *9*, 1335.
(34) Zang, D. Y.; Rio, E.; Langevin, D.; Wei, B.; Binks, B. P. Viscoelastic Properties of Silica Nanoparticle Monolayers at the Air-Water Interface. *Eur. Phys. J. E: Soft Matter Biol. Phys.,* **2010**, *31*, 125-134.
(35) Lin, B. J.; Chen, L. J. Phase Transitions in Two-Dimensional Colloidal Particle System Observed in Langmuir Trough. *Colloid Surf. A,* **2006**, *284*, 239-245.

(36) Evans, J. E.; Jungjohann, K. L.; Wong, P. C. K.; Chiu, P. L.; Dutrow, G. H.; Arslan, I.; Browning, N. D. Visualizing Macromolecular Complexes with in Situ Liquid Scanning Transmission Electron Microscopy. *Micron,* **2012**, *43*, 1085-1090.
(37) Zheng, H. M.; Claridge, S. A.; Minor, A. M.; Alivisatos, A. P.; Dahmen, U. Nanocrystal Diffusion in a Liquid Thin Film Observed by in Situ Transmission Electron Microscopy. *Nano Lett.,* **2009**, *9*, 2460-2465.
(38) Yuk, J. M.; Park, J.; Ercius, P.; Kim, K.; Hellebusch, D. J.; Crommie, M. F.; Lee, J. Y.; Zettl, A.; Alivisatos, A. P. High-Resolution Em of Colloidal Nanocrystal Growth Using Graphene Liquid Cells. *Science,* **2012**, *336*, 61-64.
(39) Costa, L.; Li-Destri, G.; Thomson, N. H.; Konovalov, O.; Pontoni, D. Real Space Imaging of Nanoparticle Assembly at Liquid-Liquid Interfaces with Nanoscale Resolution. *Nano Lett.,* **2016**, *16*, 5463-5468.
(40) Hell, S. W. Far-Field Optical Nanoscopy. *Science,* **2007**, *316*, 1153-1158.
(41) Jones, S. A.; Shim, S. H.; He, J.; Zhuang, X. W. Fast, Three-Dimensional Super-Resolution Imaging of Live Cells. *Nat. Methods,* **2011**, *8*, 499-508.
(42) Wang, D. P.; Yordanov, S.; Paroor, H. M.; Mukhopadhyay, A.; Li, C. Y.; Butt, H. J.; Koynov, K. Probing Diffusion of Single Nanoparticles at Water-Oil Interfaces. *Small,* **2011**, *7*, 3502-3507.
(43) Bonales, L. J.; Rubio, J. E. F.; Ritacco, H.; Vega, C.; Rubio, R. G.; Ortega, F. Freezing Transition and Interaction Potential in Monolayers of Microparticles at Fluid Interfaces. *Langmuir,* **2011**, *27*, 3391-3400.
(44) Lahtinen, J. M.; Hjelt, T.; Ala-Nissila, T.; Chvoj, Z. Diffusion of Hard Disks and Rodlike Molecules on Surfaces. *Phys. Rev. E,* **2001**, *64*, 021204.
(45) Ma, X. G.; Chen, W.; Wang, Z. R.; Peng, Y.; Han, Y. L.; Tong, P. E. Test of the Universal Scaling Law of Diffusion in Colloidal Monolayers. *Phys. Rev. Lett.,* **2013**, *110*, 078302.
(46) Medinanoyola, M. Long-Time Self-Diffusion in Concentrated Colloidal Dispersions. *Phys. Rev. Lett.,* **1988**, *60*, 2705-2708.
(47) Mendoza, A. J.; Guzman, E.; Martinez-Pedrero, F.; Ritacco, H.; Rubio, R. G.; Ortega, F.; Starov, V. M.; Miller, R. Particle Laden Fluid Interfaces: Dynamics and Interfacial Rheology. *Adv. Colloid Interface Sci.,* **2014**, *206*, 303-319.
(48) Ortega, F.; Ritacco, H.; Rubio, R. G. Interfacial Microrheology: Particle Tracking and Related Techniques. *Curr. Opin. Colloid Interface Sci.,* **2010**, *15*, 237-245.
(49) Schaertl, W.; Sillescu, H. Dynamics of Colloidal Hard-Spheres in Thin Aqueous Suspension Layers - Particle Tracking by Digital Image-Processing and Brownian Dynamics Computer-Simulations. *J. Colloid Interface Sci.,* **1993**, *155*, 313-318.
(50) Thorneywork, A. L.; Aarts, D. G. A. L.; Horbach, J.; Dullens, R. P. A. Self-Diffusion in Two-Dimensional Binary Colloidal Hard-Sphere Fluids. *Phys. Rev. E,* **2017**, *95*, 012614.
(51) Vanmegen, W.; Underwood, S. M. Tracer Diffusion in Concentrated Colloidal Dispersions .3. Mean Squared Displacements and Self-Diffusion Coefficients. *J. Chem. Phys.,* **1989**, *91*, 552-559.
(52) Zahn, K.; MendezAlcaraz, J. M.; Maret, G. Hydrodynamic Interactions May Enhance the Self-Diffusion of Colloidal Particles. *Phys. Rev. Lett.,* **1997**, *79*, 175-178.
(53) Dörr, A.; Hardt, S.; Masoud, H.; Stone, H. A. Drag and Diffusion Coefficients of a Spherical Particle Attached to a Fluid-Fluid Interface. *J. Fluid Mech.,* **2016**, *790*, 607-618.

(54) Krieger, I. M.; Dougherty, T. J. A Mechanism for Non-Newtonian Flow in Suspensions of Rigid Spheres. *Trans. Soc. Rheol.* **1959**, *3*, 137-152.
(55) Mishra, C. K.; Rangarajan, A.; Ganapathy, R. Two-Step Glass Transition Induced by Attractive Interactions in Quasi-Two-Dimensional Suspensions of Ellipsoidal Particles. *Phys. Rev. Lett.,* **2013**, *110*, 188301.
(56) Prasad, V.; Koehler, S. A.; Weeks, E. R. Two-Particle Microrheology of Quasi-2d Viscous Systems. *Phys. Rev. Lett.* **2006**, *97*, 176001.
(57) Donev, A.; Torquato, S.; Stillinger, F. H.; Connelly, R. Jamming in Hard Sphere and Disk Packings. *J. Appl. Phys.,* **2004**, *95*, 989-999.
(58) Gao, Y. G.; Kim, P. Y.; Hoagland, D. A.; Russell, T. P. Bidisperse Nanospheres Jammed on a Liquid Surface. *ACS Nano,* **2020**, *14*, 10589-10599.
(59) Brock, J. D.; Strandburg, K. J.; Bond-Orientational Order. In Bond-Orientational Order in Condensed Matter Systems; Strandburg, K. J. Ed. Springer US, 2012, pp 1-77.
(60) Choudhury, S.; Agrawal, A.; Kim, S. A.; Archer, L. A. Self-Suspended Suspensions of Covalently Grafted Hairy Nanoparticles. *Langmuir,* **2015**, *31*, 3222-3231.
(61) Liu, X. T.; Abel, B. A.; Zhao, Q.; Li, S. K.; Choudhury, S.; Zheng, J. X.; Archer, L. A. Microscopic Origins of Caging and Equilibration of Self-Suspended Hairy Nanoparticles. *Macromolecules,* **2019**, *52*, 8187-8196.
(62) Kharel, A.; Lodge, T. P. Effect of Ionic Liquid Components on the Coil Dimensions of Peo. *Macromolecules,* **2019**, *52*, 3123-3130.
(63) Salerno, K. M.; Ismail, A. E.; Lane, J. M. D.; Grest, G. S. Coating Thickness and Coverage Effects on the Forces between Silica Nanoparticles in Water. *J. Chem. Phys.,* **2014**, *140*, 194904.
(64) Huerre, A.; Cacho-Nerin, F.; Poulichet, V.; Udoh, C. E.; De Corato, M.; Garbin, V. Dynamic Organization of Ligand-Grafted Nanoparticles During Adsorption and Surface Compression at Fluid-Fluid Interfaces. *Langmuir,* **2018**, *34*, 1020-1028.
(65) Torquato, S.; Truskett, T. M.; Debenedetti, P. G. Is Random Close Packing of Spheres Well Defined? *Phys. Rev. Lett.,* **2000**, *84*, 2064-2067.
(66) Ethier, J. G.; Hall, L. M. Structure and Entanglement Network of Model Polymer-Grafted Nanoparticle Monolayers. *Macromolecules,* **2018**, *51*, 9878-9889.
(67) Dozier, W. D.; Lindsay, H. M.; Chaikin, P. M. Self-Diffusion in Interacting Colloidal Liquids. *J. Phys. Colloques,* **1985**, *46*, 165-172.

TOC

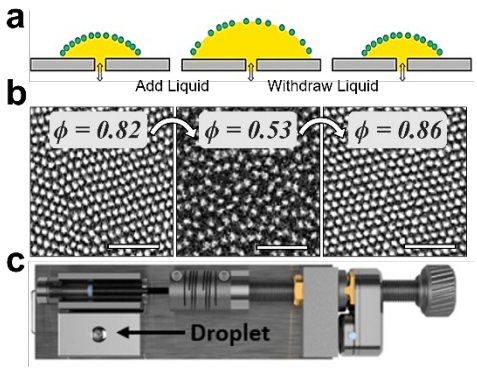
a
Add Liquid
Withdraw Liquid
b
$\phi = 0.82$
$\phi = 0.53$
$\phi = 0.86$
c
Droplet